Tuning the Piezoelectric Fields in Quantum Dots: Microscopic Description of Dots Grown on $(N11)$ Surfaces

Michael Povolotskyi, Aldo Di Carlo, Paolo Lugli, Stefan Birner, and Peter Vogl

***Abstract*—We theoretically investigated the elastic deformation and piezoelectric field in InAs quantum dots grown on $(N11)$ GaAs substrates. Particular attention was given to the influence of the substrate orientation on both the volume deformation of the dot and the strain-induced piezoelectric field. The piezoelectric effects are enhanced by the lower symmetry growth directions. The influence of the piezoelectric fields on the electron and hole ground states for a $(N11)$ quantum dot was also investigated within the effective mass approximation. We find a significant dependence of the fundamental transition energy on the polarity of the substrate's surface.**

***Index Terms*—Piezoelectricity, quantum dot, strain.**

I. Introduction

RECENT advances in growth techniques have made semiconducting quantum dots (QD) grown along $[N11]$ directions a reality [1]. In contrast to the traditional (001) orientation, this geometry enables significant piezoelectric fields in the case of polar crystals with the zinc-blende structure, such as GaAs, AlAs, InAs, and their alloys. These fields lead to a quantum confined stark effect, which efficiently affects the optical properties of $(N11)$ oriented devices [2]. Consequently, an increasing number of experimental studies has been devoted to such promising systems [3], [4]. Yet, due to the complex geometry of $(N11)$ oriented structures, few theoretical investigations have been performed in this domain.

Heterostructures, made of materials with different lattice constants, are subjected to elastic deformations. In the case of (001) oriented systems, such deformations have been studied in the framework of both the continuum mechanical model [5], [6] and the valence force field model [7]. Piezoelectric effects, which occur in zinc-blende crystals in the presence of a shear deformation were also theoretically investigated for quantum wells (QWs) [8], [9], quantum wires (QWRs) [10], and quantum dots (QDs) [11]. A number of theoretical studies were devoted to the electronic properties of semiconductor nanostructures. They were performed in the framework of the envelope function approximations [11], as well as in more refined approaches developed recently, such as the empirical tight-binding method [12], [13] or the empirical pseudopotential method [14]. The electronic structure of GaAs/AlGaAs $[N11]$ oriented superlattices and unstrained quantum wires was studied in the framework of $\mathbf{k}\cdot\mathbf{p}$ theory [15], [16]. In a similar approximation, the effect of strain on the optical properties of a bulk $[N11]$-oriented system was studied by Henderson and Towe [17].

In this paper, we focus on the influence of strain and piezoelectric fields on the electronic properties of $(N11)$ oriented QDs. The paper is organized as follows. In Section II, we describe the physical model and methods of numerical calculations, which we apply in Section III to particular examples of a QD; Section IV summarizes our results.

Manuscript received September 23, 2003; revised October 1, 2003. This work was supported in part by the Office of Naval Research and in part by the PAIS-PIE Project.

M. Povolotskyi, A. Di Carlo, and P. Lugli are with the Department of Electrical Engineering, University of Rome, 00133 Rome, Italy (e-mail: povolotskyi@ing.uniroma2.it).

S. Birner and P. Vogl are with the Walter Schottky Institute and the Physics Department, Technical University of Munich, 85748 Garching, Germany.

Digital Object Identifier 10.1109/TNANO.2003.820819

II. Theory

A. Elastic Deformations and Piezoelectric Fields

We calculated the elastic deformation of our model structures by using a continuous medium model [5], [6]. In this approach, we consider the small displacements of the material points $\mathbf{u}(\mathbf{x})$, which are derived from the local tensor $A_{ij} = \partial u_i/\partial x_j$. Since only the symmetric part of A_{ij} describes "pure" deformations without rotation, the strain tensor ε_{ij} is defined as

$$\varepsilon_{ij} = \frac{1}{2}\left(A_{ij} + A_{ji}\right). \tag{1}$$

As for the boundary conditions, we use the mechanical equilibrium condition, written for the case of vanishing external forces

$$\frac{\partial \sigma_{ij}}{\partial x_i} = \mathbf{0} \tag{2}$$

where σ_{ij} is the stress tensor, which is related to the strain tensor (1) by Hooke's law

$$\sigma_{ij} = C_{ijkl}\cdot\varepsilon_{kl}. \tag{3}$$

The tensor C_{ijkl}, referred to as elasticity tensor, is a bulk material property. It is usually defined in the crystallographic coordinate system, but in our case it is more convenient to work in a "growth-oriented" basis whose z axis is parallel to the growth direction. This new set of coordinate axes is, in the case of $(N11)$ structures

$$\begin{aligned}\mathbf{x} &= [0,1,\bar{1}]\\ \mathbf{y} &= [2,\bar{N},\bar{N}]\\ \mathbf{z} &= [N,1,1].\end{aligned} \tag{4}$$

1536-125X/04$20.00 © 2004 IEEE

With this choice, the elasticity tensor must be transformed to the new system (4) according to the rule

$$C_{ijkl} = R_{ii'}R_{jj'}R_{kk'}R_{ll'}C_{i'j'k'l'} \tag{5}$$

where R_{ij} is a rotation matrix whose rows are equal to the normalized basis vectors (4). For materials with cubic symmetry, it can be shown that the resulting elasticity tensor has eight zero components among its 21 independent ones. These are namely C_{xxxz}, C_{yyxz}, C_{zzxz}, C_{yzxz}, C_{xxxy}, C_{yyxy}, C_{zzxy}, and C_{yzxy}.

In order to define the model QD structure, which consists of materials with different lattice constants, we assume a coherent growth, so that all distinct lattices are perfectly matched at the interface [9]. We used the following computational procedure in order to solve (2), while imposing the lattice matching conditions. First we map a rectangular nonhomogeneous simulation grid over the whole structure in such a way that all the material interfaces coincide with the grid lines; we then introduce a "lattice matching" deformation which transforms any unstrained unit cell of the QD material in order to match it to the substrate material's lattice:

$$\tilde{\varepsilon}_{ij}(\mathbf{x}) = \frac{1}{2}\left(\frac{\partial \tilde{u}_i}{\partial x_j} + \frac{\partial \tilde{u}_j}{\partial x_i}\right) + W(\mathbf{x})\delta_{ij}\frac{a_S - a_D}{a_D} \tag{6}$$

$$W(\mathbf{x}) = \begin{cases} 1, & \text{if } \mathbf{x} \text{ belongs to the QD or wetting layer} \\ 0, & \text{otherwise} \end{cases} \tag{7}$$

where the $\tilde{\mathbf{u}}$ are the displacements additional to the "lattice matching" deformations, and a_S and a_D are the substrate and QD lattice constants, respectively. Finally, the equation of equilibrium (2) takes the following form:

$$\frac{\partial \tilde{\sigma}_{ij}}{\partial x_i} = 0 \tag{8}$$

where $\tilde{\sigma}_{ij} = C_{ijkl}\tilde{\varepsilon}_{kl}$. Equation (8) is a partial differential equation of the second order with respect to the displacements $\tilde{\mathbf{u}}(\mathbf{x})$. It is discretized by using the box integration method and reduced to a linear system with a sparse matrix.

We then calculated the piezoelectric polarization, which is linearly related to strain

$$P_i = e_{ijk}\varepsilon_{jk} \tag{9}$$

where the e_{ijk} are the piezoelectric tensor components. Due to the cubic symmetry of zinc-blende crystals, the nonzero e_{ijk}'s, in the crystallographic coordinate system, are only related to shear deformations. In the coordinate system (4), however, diagonal components of the strain tensor may also contribute to the piezoelectric polarization. In this paper, we neglect the converse piezoelectric effect [18], and use the polarization $\mathbf{P}$ to obtain the electric potential from the Poisson equation

$$-\nabla(\kappa\nabla\varphi) = -\nabla\mathbf{P} \tag{10}$$

where κ is the dielectric constant. Here, we consider that there are no free charges in the structure, thus the built-in electric field may originate only from a piezoelectric charge $\rho_{\text{piezo}} = -\nabla\mathbf{P}$.

B. Electron and Hole Eigenstates

We investigated the electron and hole eigenstates in our model QD structures within the effective mass approximation (EMA), and considered only the lowest conduction band for electrons and the highest valence band for holes. Strain-induced shifts of the conduction band depend only on the hydrostatic part of the strain: $\delta E_c = -a_c\text{Tr}(\varepsilon_{ij})$. Here, the influence of strain on the electron effective mass was neglected and, therefore, an isotropic effective mass was considered. The band shifts and the effective mass tensor for the highest valence band are obtained from the Bir–Pikus 6×6 $\mathbf{k}\cdot\mathbf{p}$ Hamiltonian [17], [19]. In our approach, the hole effective mass is position dependent. At a given $\mathbf{r}$ point, $m^*(\mathbf{r})$ is the effective mass of the bulk semiconductor, subjected to the homogeneous strain $\varepsilon(\mathbf{r})$. The electron and hole eigenstates were obtained as the solutions of the one-particle Schrödinger equation:

$$\left(-\frac{\hbar^2}{2}\frac{\partial}{\partial x_i}\frac{1}{m^*_{ij}(\mathbf{r})}\frac{\partial}{\partial x_j} + V_\varepsilon(\mathbf{r}) + q\varphi(\mathbf{r})\right)\psi = E\psi \tag{11}$$

where m^*, q, V_ε, φ are the conduction (valence) band effective mass, electron (hole) charge, conduction (valence) band edge energy, and piezoelectric potential, respectively. Equation (11) is discretized over a rectangular nonhomogeneous grid by using the box integration method. The problem is then reduced to the diagonalization of a Hermitian sparse matrix.

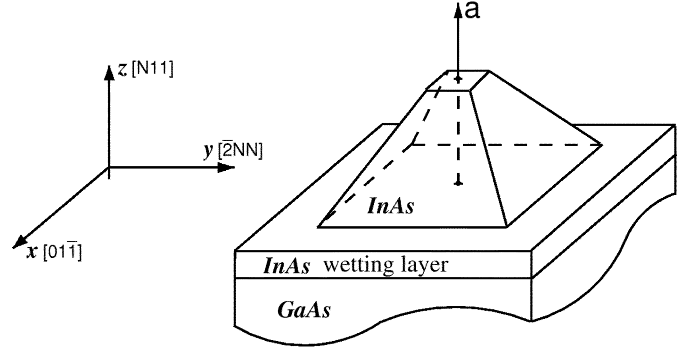

Fig. 1. Schematic drawing of our model system: quantum dot, WL, and substrate.

III. Results and Discussion

We consider as our model system an InAs quantum dot structure grown on an $[N11]$-oriented $(N = 1, 2, \ldots)$ GaAs substrate. The dot has the shape of a symmetric truncated tetrahedral pyramid, standing on a wetting layer (WL), embedded in a GaAs matrix (see Fig. 1). The two bases of the pyramid are squares of a size 10×10 nm and 2×2 nm. The WL thickness is 1 nm, and the dot height is 4 nm. The theoretical approach presented here has been implemented in Next**nano**^{3} software [20]. The material parameters were taken from [21]. Note that more complex but still pyramidal shapes were reported by Temko *et al.* for InAs/GaAs dots grown by molecular-beam epitaxy [22].

A. Strain Distribution in a QD

Contour plots of the diagonal strain components in two perpendicular cross sections are shown in Fig. 3, for the [211] growth direction. The results are qualitatively the same for any $[N11]$-like direction. The plots indicate that both the QD and WL materials are compressed in the x and y directions (ε_{yy}, ε_{xx} are negative), in agreement with the relative values of the lattice

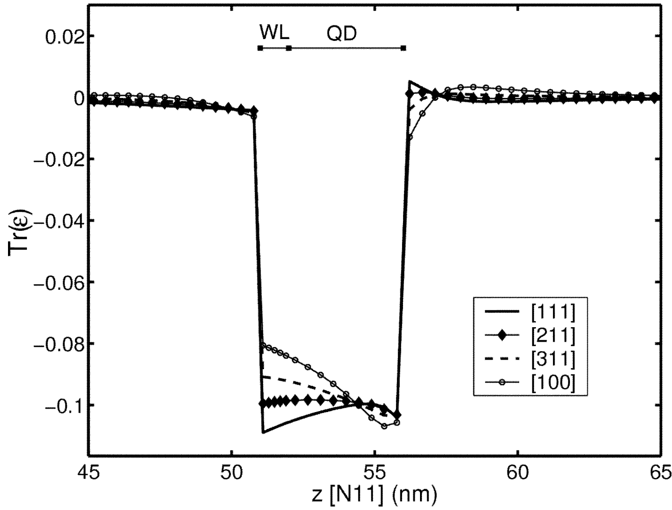

Fig. 2. $Tr(\varepsilon_{ij})$ along the QD symmetry axis a (see Fig. 1) calculated for four different orientations of the substrate: (111), (211), (311), and (100). The WL and QD location is indicated.

constants of InAs and GaAs. As far as the ε_{zz} is concerned, the situation is quite different: whereas the two-dimensional WL is tensile stressed in the growth direction, the QD region is compressed, because the lateral faces of the pyramid are also subjected to the compression. Interestingly, the strain distribution is symmetric in the $(\bar{1}11)$ plane [Fig. 3(b)] and is not symmetric in the $(0\bar{1}1)$ plane, despite the symmetric QD shape [Fig. 3(a)]. The loss of symmetry in the latter case is due to the fact that the $[N11]$ and $[\bar{2}NN]$ directions do not coincide with the high-symmetry axes of a cubic crystal. Still, for any structure having a symmetry plane perpendicular to the $[0\bar{1}1]$ axis, the ε_{xx}, ε_{yy}, ε_{zz}, and ε_{yz} components of the strain tensor are even functions with respect to the $\mathbf{x} \rightarrow -\mathbf{x}$ transformation [see Fig. 3(b)], whereas ε_{xy} and ε_{xz} are odd functions.

In order to compare the strain distribution for different growth directions, we plotted $Tr(\varepsilon)$ along QD symmetry axis for $(N11)$ $(N = 1, 2, 3)$ and (001) substrate orientations (see Fig. 2). The last case corresponds to $N = \infty$. In the case of the $[001]$ growth direction, the WL is less compressed than the pyramid. With the reduction of N, the WL is getting more stressed, and in the limiting case of the $[111]$ growth direction, it is compressed even more than the QD. Thus, it is possible to "relax" the QD region with respect to the WL by varying its growth direction. Such a behavior is due to the difference in the elasticity modules for different bases [see (5)].

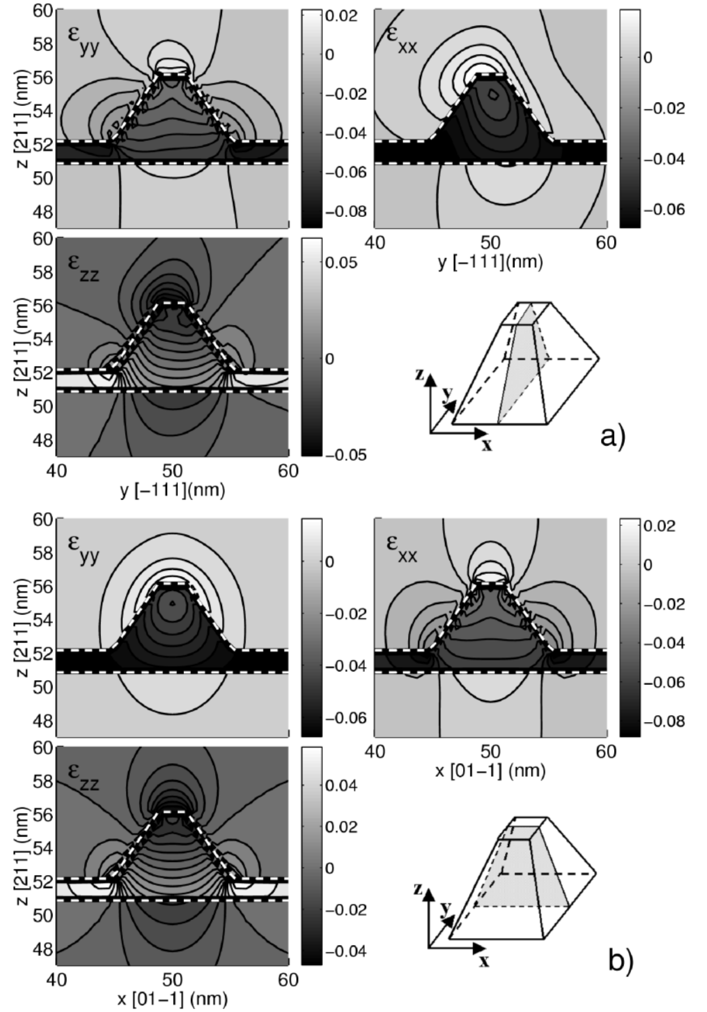

Fig. 3. Distribution of the diagonal strain components in two perpendicular QD cross sections. The intersecting planes, schematically shown in the right lower corners, have $(01\bar{1})$ and $(\bar{1}11)$ crystallographic orientation, respectively. Both planes contain the QD symmetry axis a (see Fig. 1). InAs/GaAs interfaces are indicated by white dashed lines.

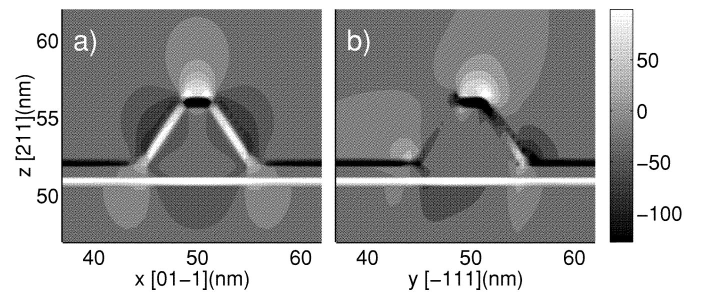

Fig. 4. Contour plot of the piezoelectric charge density in the two cross sections of a QD: a) $(\bar{1}11)$-plane and b) $(01\bar{1})$-plane (see Fig. 3). The QD is grown on (211)-oriented A-type substrate (see text). The units are 10^{18} e/cm^3.

B. Piezoelectric Fields in a QD

The piezoelectric charge density, calculated for a (211) oriented QD, is shown in Fig. 4. Due to the nature of the piezoelectric effect, the sign of the piezoelectric charge depends on the atomic composition of the interfaces [2]. We thus have to distinguish between the substrate's Ga planes, referred to as $(N11)$ A-plane, and the As planes, referred to as $(N11)$ B-plane. From the computational point of view, these two cases differ in the sign of the piezoelectric tensor e_{ijk} [see (9)]. In Fig. 4, the charge density is plotted for a (211)A substrate. There are two reasons for the piezoelectric charge existence, namely, the discontinuity of the piezoelectric constant at the interfaces and the nonzero gradient of strain. This explains the big charge density at the interfaces that corresponds to a surface charge. In addition, there is a volume charge inside the QD, where the strain is highly nonhomogeneous. We find that the piezo-charge distribution in a $(N11)$ QD has a dipole symmetry, rather than the quadrupole symmetry that was reported by Stier *et al.* [11] for a (100) oriented QD.

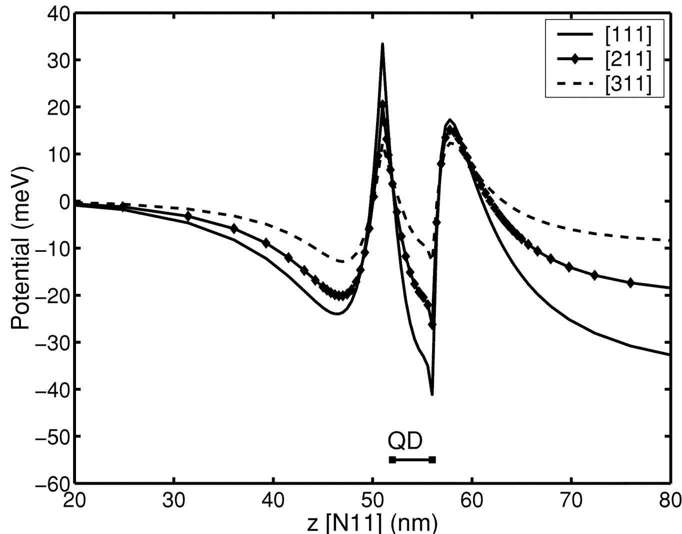

Fig. 5. Piezoelectric potential along the QD symmetry axis a (see Fig. 1) calculated for three different orientations of the substrate: (111) A, (211) A and (311) A. The QD location is shown.

In Fig. 5, we show the piezoelectric potential dependence on the growth directions N (the potential is calculated along a QD symmetry axis). We note that the piezoelectric field has the highest magnitude for the (111)A growth direction. The field gets smaller with increasing N, and finally vanishes for the case of the (100) growth direction (not shown here).

C. Electron and Hole States

Our model enables us to consider two effects on the electron and hole states, namely, the effect of strain and the effect of the piezoelectric charge. The effect of strain in our model does not depend on the substrate termination type, but the piezo effect does. In order to estimate the role of the piezoelectric field, we calculated the fundamental transition energy without any piezoelectric field, and with the field for both the A and B substrate type (see Table I). The energy shift due to the piezoelectric field has a different magnitude for the case A and B substrate termination. This is because the electric field can increase or decrease the electron/hole space separation that already exists due to the strain. This shift is negligible (less than 1 meV) for (100)-oriented structures and reaches a value of more than 10 meV for [111] orientations.

The energy shift reported by Sanguinetti *et al.* [2] is always positive, regardless of a substrate type. The discrepancy is, probably, an evidence of the fact that the geometry of experimentally investigated QDs is different from the model one. Always positive energy shift can occur if the effect of piezoelectric field on the electron/hole separation is dominant with the respect to the effect of strain and geometry. Also, our model could be made more exact by considering of a band-mixing effect for the hole state description. This could be done, for example, in the framework of $\mathbf{k}\cdot\mathbf{p}$ perturbation theory. We expect that the main effect of the light hole band included in the basis would be a slight lowering of the hole eigenenergy.

TABLE I
FUNDAMENTAL TRANSITION ENERGY (EV)

Growth direction	No piezoeffect	(N11)A	(N11)B
[111]	1.254	1.262	1.241
[211]	1.241	1.243	1.233
[311]	1.224	1.226	1.221
[100]	1.205	1.205	1.205

IV. CONCLUSION

We investigated the structural and electronic properties of InAs QD systems grown on $(N11)$ oriented GaAs substrates. We obtained a nonsymmetric strain pattern, as well as an increasing piezoelectric field, for high-index orientations. Our calculations also demonstrate that by varying the growth direction and the substrate termination type, it is possible to tailor the built-in electric field, and, therefore, the optical transition energy of these QD systems.

ACKNOWLEDGMENT

The authors acknowledge many useful discussions with Dr. J. Gleize.

REFERENCES

[1] P. P. Gonzálcs-Borrero *et al.*, "Self-organized InGaAs quantum dots grown by molecular beam epitaxy on (100), (711)A/B, (511)A/B, (311)A/B, (211)A/B, and (111)A/B oriented GaAs," *J. Crystal Growth*, vol. 169, pp. 424–428, 1996.
[2] S. Sanguinetti, M. Gurioli, E. Grilli, M. Guzzi, and M. Henini, "Piezoelectric-induced quantum-confined stark effect in self-assembled InAs quantum dots grown on $(N11)$ GaAs substrates," *Appl. Phys. Lett.*, vol. 77, pp. 1982–1984, 2000.
[3] S. Marcinkevičius, J. Siegert, R. Leon, B. Čechavičius, B. Magness, W. Taylor, and C. Lobo, "Changes in luminescence intensities and carrier dynamics induced by proton irradiation in $\mathrm{In}_x\mathrm{Ga}_{1-x}\mathrm{As}/\mathrm{GaAs}$ quantum dots," *Phys. Rev. B*, vol. 66, pp. 235314–235314-6, 2002.
[4] S. Frechengues *et al.*, "Wavelength tuning of InAs quantum dots grown on (311)B InP," *Appl. Phys. Lett.*, vol. 74, pp. 3356–3358, 1999.
[5] C. Pryor, M.-E. Pistol, and L. Samuelson, "Electronic structure of strained $\mathrm{InP}/\mathrm{Ga}_{0.51}\mathrm{In}_{0.49}\mathrm{P}$ quantum dots," *Phys. Rev. B*, vol. 56, pp. 10404–10411, 1997.
[6] B. Jogai, "Three-dimensional strain field calculations in coupled InAs/GaAs quantum dots," *J. Appl. Phys.*, vol. 88, pp. 5050–5055, 2000.
[7] P. N. Keating, "Effect of invariance requirements on the elastic strain energy of crystals with application to the diamond structure," *Phys. Rev.*, vol. 145, pp. 637–645, 1966.
[8] D. Smith and C. Mailhiot, "Piezoelectric effects in strained-layer superlattices," *J. Appl. Phys.*, vol. 63, pp. 2717–2719, 1988.
[9] L. De Caro and L. Tapfer, "Elastic lattice deformation of semiconductor heterostructures grown on arbitrarily oriented substrated surfaces," *Phys. Rev. B*, vol. 48, pp. 2298–2303, 1993.
[10] L. D. Caro and L. Tapfer, "Strain and piezoelectric fields in arbitrarily oriented semiconductor heterostructures II. Quantum wires," *Phys. Rev. B*, vol. 51, pp. 4381–4387, 1995.
[11] O. Stier, M. Grundmann, and D. Bimberg, "Electronic and optical properties of strained quantum dots modeled by 8-band kp theory," *Phys. Rev. B*, vol. 59, pp. 5688–5701, 1998.
[12] A. Di Carlo, "Microscopic theory of nanostructured semiconductor devices: Beyond the envelope-function approximation," *Semicond. Sci. Technol.*, vol. 18, pp. R1–R31, 2003.
[13] G. Klimeck, F. Oyafuso, R. C. Bowen, and T. B. Boykin, "3-D atomistic nanoelectronic modeling on high performance clusters: Multimillion atom simulations," *Superlattices and Microstructures*, vol. 31, pp. 171–179, 2002.

[14] A. J. Williamson, L. W. Wang, and A. Zunger, "Theoretical interpretation of the experimental electronic structure of lens-shaped self-assembled InAs/GaAs quantum dots," *Phys. Rev. B*, vol. 62, pp. 12963–12977, 2000.
[15] J.-B. Xia, "Effective-mass theory for superlattices grown on (11N)-oriented substrates," *Phys. Rev. B*, vol. 43, pp. 9856–9864, 1991.
[16] S.-S. Li and J.-B. Xia, "Effective-mass theory for $\mathrm{GaAs/Ga_{1-x}Al_xAs}$ quantum wires and corrugated superlattices grown on (311)-oriented substrates," *Phys. Rev. B*, vol. 50, pp. 8602–8608, 1994.
[17] R. H. Henderson and E. Towe, "Strain and crystallographic orientation effects on interband optical matrix elements and band gaps of $[11l]$-oriented III-V epilayers," *J. Appl. Phys.*, vol. 78, p. 2447, 1995.
[18] T. B. Bahder, "Converse piezoelectric effect in $[111]$ strained layer heterostructures," *Phys. Rev. B*, vol. 51, pp. 10892–10896, 1995.
[19] C. Y.-P. Chao and S. L. Chuang, "Spin-orbit-coupling effects on the valence-band structure of strained semiconductor quantum wells," *Phys. Rev. B*, vol. 46, pp. 4110–4122, 1992.
[20] Next**nano**^{3} Device Simulation Package [Online]. Available: http://www.nextnano.de
[21] I. Vurgaftman, J. R. Meyer, and L. R. Ram-Mohan, "Band parameters for III-V compound semiconductors and their alloys," *J. Appl. Phys.*, vol. 89, pp. 5815–5875, 2001.
[22] Y. Temko, T. Suzuki, and K. Jacobi, "Shape and growth of InAs quantum dots on GaAs(113)A," *Appl. Phys. Lett.*, vol. 82, pp. 2142–2144, 2003.

Michael Povolotskyi was born in Cherkassy, Ukraine, in 1977. He received the M.S. degree in applied mathematics and physics from the Moscow Institute of Physics and Technology, Moscow, Russia, in 2000. He is currently working toward the Ph.D. degree in the Department of Electronic Engineering, University of Rome "Tor Vergata," Rome, Italy.

His current research is focused on the theoretical study of electronic and optical properties of semiconductor structures.

Aldo Di Carlo received the physics degree from the University of Rome, Rome, Italy, in 1991, and the Ph.D. degree from the Walter Schottky Institute of the Technical University, Munich, Germany, in 1995.

He is currently an Associate Professor in the Department of Electronic Engineering, University of Rome "Tor Vergata," Rome, Italy, where his research interests include the theoretical study of optical and transport processes in semiconductor nanostructures, devices, and organic materials.

Paolo Lugli was born in Carpi, Italy, in 1956. He received the Laurea degree in physics from the University of Modena, Modena, Italy, in 1979, and the Ph.D. degree in electrical engineering from Colorado State University, Fort Collins, in 1985.

He is currently a Full Professor of optoelectronics at the University of Rome "Tor Vergata," Rome, Italy. His current research interests include the theoretical study and numerical simulation of semiconductor nanostructures and devices.

Stefan Birner was born in Hirschau, Germany, in 1975. He received the Vordiplom degree in physics from the University of Bayreuth, Bayreuth, Germany, and the Master of Physics degree from the University of Exeter, Exeter, U.K. in 2000. He is currently working toward the Ph.D. degree at the Walter Schottky Institute, Technical University of Munich, Munich, Germany.

In 2000, he was with the Physics Department, The Ohio State University, Columbus, where he performed molecular dynamics studies of defects in Si.

Mr. Birner is a Member of the Student MemberChip Program of Infineon Technologies.

Peter Vogl was born in Graz, Austria, in 1949. He received the Ph.D. degree in physics from the University of Graz, Graz, Austria, in 1974.

Since 1990, he has been a Professor for Theoretical Semiconductor Physics, at the Walter Schottky Institute, Technical University of Munich, Munich, Germany, and the Physics Department of the Technical University of Munich, Garching, Germany. His current research interests include the electronic structure and charge carrier transport in semiconductors, ferroelectrics, magnetic materials, and conducting polymers.